Optica Applicata, Vol. XLIII, No. 2, 2013
DOI: 10.5277/oa130205

Focus shaping of Weierstrass solid immersion lens by an axisymmetric Bessel-modulated Gaussian beam

XIANGMEI DONG*, TAO GENG, SONGLIN ZHUANG

Engineering Research Center of Optical Instrument and System,
Ministry of Education and Shanghai Key Lab of Modern Optical System,
University of Shanghai for Science and Technology,
No. 516 JunGong Road, Shanghai 200093, China

*Corresponding author: mmsoap@163.com

Weierstrass solid immersion lens (SIL) has been used to obtain superresolution because a smaller focal size is desirable. In this paper, focus shaping of Weierstrass SIL illuminated by an axisymmetric Bessel-modulated Gaussian beam (QBG beam) is investigated. It has been found theoretically that the sharper focusing of Weierstrass SIL disappears for a certain beam order of QBG beam. For case of a smaller beam order, the focus still locates on the plane of Weierstrass SIL and Weierstrass SIL still plays a tighter focusing role. However, when the beam order increases continuously, the focus lefts the plane of Weierstrass SIL, and shifts along an optical axis considerably. In addition, under condition of the higher beam order, the dependence of the focal shift on the beam order is nearly linear, which may be used to alter a focal position conveniently.

Keywords: Weierstrass solid immersion lens, Bessel-modulated Gaussian beam, vector diffraction theory.

1. Introduction

Focus size is a very important parameter in many optical systems, and it is usually known that a focal spot size is about $\lambda/2\mathrm{NA}$, where λ is the wavelength of the laser light and $\mathrm{NA} = n\sin(\alpha)$ is the numerical aperture (NA) of the system, where n is the refractive index of the material, and α is the convergence angle of the lens [1]. Therefore, a smaller focal size may be decreased by increasing the NA, shortening λ, or increasing n. Therefore, a solid immersion lens (SIL) was used to decrease the size of a focal spot [2]. There are two types of spherical SILs, one is a simple hemisphere SIL [2] and the other is an aplanatic supersphere SIL (Weierstrass optic) [3]. Because NA may be improved by a factor of n^2, the Weierstrass SIL has widely been applied in optical storage [3, 4], lithography [5], light extraction [6], surface microscopy [7] and subsurface microscopy [8], and spectroscopic imaging of semiconductor nanostructures [9]. Focal size within $\lambda/10$ at the bottom of the hemisphere SIL can be achieved [10, 11].

On the other hand, since CARON and POTVLIEGE introduced a novel class of beams expressed in a cylindrical coordinate system, namely, the Bessel-modulated Gaussian beams with quadratic radial dependence (QBG beam) [12], QBG beam has attracted much attention [13–15]. It was shown that such class of beams has familiar collinear geometry of the Gaussian beam and also interesting non-Gaussian features for certain values of its parameters [12]. Particularly, it was demonstrated that the zeroth-order QBG beam, which is referred to as the axisymmetric QBG beam, can be expanded in Laguerre–Gauss modes and has a very flat axial profile when the beam parameter l is of order of unity [12, 13]. Bessel-modulated Gaussian light beams passing through a paraxial ABCD optical system with an annular aperture have also been studied [16]. Focusing properties of the cylindrical vector and the spiral polarized axisymmetric QBG beam were also studied by the vector diffraction theory [17–19].

However, to our knowledge, the focusing properties of QBG beam through Weierstrass SIL have not been investigated. The aim of this paper is to get deep insight into the effect of Weierstrass SIL, so we studied the focus shaping of Weierstrass SIL illuminated by QBG beam, and found that Weierstrass SIL still plays a tighter focusing role for case of a smaller beam order. When the beam order increases continuously, focus lefts the plane of Weierstrass SIL, and shifts along an optical axis considerably. The principle of the focusing QBG beam through Weierstrass SIL is given in Section 2. Section 3 shows the simulation results and discussions. The conclusions are summarized in Section 4.

2. Focusing principle of Bessel-modulated Gaussian beam through Weierstrass SIL

Weierstrass SIL is placed in a laser path with the focus on its plane surface. The Weierstrass SIL's thickness is $R(1 + 1/n)$, where R is its radius and n is the refractive index of the material. We assume that the system is illuminated by the axisymmetric QBG beam with polarization in x coordinate direction. Following the procedure similar to that in references [20, 21], we can obtain the transmitted field distribution near the focus of the aplanatic Weierstrass SIL in the form,

$$\mathbf{E}(r,\ \varphi,\ z) = E_x(r,\ \varphi,\ z)\mathbf{e}_x + E_y(r,\ \varphi,\ z)\mathbf{e}_y + E_z(r,\ \varphi,\ z)\mathbf{e}_z \tag{1}$$

where $\mathbf{e}_x$, $\mathbf{e}_y$ and $\mathbf{e}_z$ are the unit vectors in x, y and z coordinate directions, respectively; $(r,\ \varphi,\ z)$ are the cylindrical coordinates in image space with the center at the geometric focus. The three orthogonal components can be written as [20],

$$E_x(r,\ \varphi,\ z) = I_0(u,\ v) + I_2(u,\ v)\cos(2\varphi) \tag{2a}$$

$$E_y(r,\ \varphi,\ z) = I_2(u,\ v)\sin(2\varphi) \tag{2b}$$

$$E_z(r,\ \varphi,\ z) = -2iI_1(u,\ v)\cos(2\varphi) \tag{2c}$$

where (u, v) are the axial and transverse optical coordinates and can be given by

$$u = 4nkz\sin^2(\theta_{2m}/2) \tag{3}$$

$$v = nkr\sin(\theta_{2m}) \tag{4}$$

where k is the wave number in vacuum, and θ_{2m} is the effective convergence angle that is related to the convergence angle of the objective lens α through $\theta_{2m} = \text{asin}[n\sin(\alpha)]$. The functions $I_j(u, v)$ with $j = 0, 1, 2$ are integrals over the effective aperture of the system, and are given as [20, 21],

$$I_0(u, v) = \int_0^{\theta_{2m}} A_{0x} J_0\left(\frac{v\sin(\theta_2)}{\sin(\theta_{2m})}\right) \exp\left(\frac{iu\cos(\theta_3)}{4n\sin^2\left(\frac{\theta_{2m}}{2}\right)}\right) \mathrm{d}\theta_2 \tag{5a}$$

$$I_1(u, v) = \int_0^{\theta_{2m}} A_{1x} J_1\left(\frac{v\sin(\theta_2)}{\sin(\theta_{2m})}\right) \exp\left(\frac{iu\cos(\theta_3)}{4n\sin^2\left(\frac{\theta_{2m}}{2}\right)}\right) \mathrm{d}\theta_2 \tag{5b}$$

$$I_2(u, v) = \int_0^{\theta_{2m}} A_{2x} J_2\left(\frac{v\sin(\theta_2)}{\sin(\theta_{2m})}\right) \exp\left(\frac{iu\cos(\theta_3)}{4n\sin^2\left(\frac{\theta_{2m}}{2}\right)}\right) \mathrm{d}\theta_2 \tag{5c}$$

where

$$A_{0x} = P(\theta_2)\sin(\theta_2)\left[t_{1s}t_{2s} + t_{1p}t_{2p}\cos(\theta_3)\right] \tag{6a}$$

$$A_{1x} = P(\theta_2)t_{1p}t_{2p}\sin(\theta_2)\sin(\theta_3) \tag{6b}$$

$$A_{2x} = P(\theta_2)\sin(\theta_2)\left[t_{1s}t_{2s} - t_{1p}t_{2p}\cos(\theta_3)\right] \tag{6c}$$

where $\theta_3 = \text{asin}(n\sin(\theta_2))$, and $P(\theta_2)$ is an effective apodization function; J_n is the Bessel function of the first kind of order n, (t_{1s}, t_{1p}) and (t_{2s}, t_{2p}) are the Fresnel coefficients at the spherical and planar interfaces of the Weierstrass SIL, respectively, and in the form as,

$$t_{1s} = \frac{2\cos(\theta_2)}{\cos(\theta_2) + n\cos(\beta)}, \qquad t_{1p} = \frac{2\cos(\theta_2)}{n\cos(\theta_2) + \cos(\beta)} \tag{7a}$$

$$t_{2s} = \frac{2n\cos(\theta_2)}{n\cos(\theta_2) + \cos(\theta_3)}, \qquad t_{2p} = \frac{2n\cos(\theta_2)}{\cos(\theta_2) + n\cos(\theta_3)} \tag{7b}$$

where

$$\beta = \operatorname{asin}\left[\frac{\sin(\theta_2)}{n}\right] \tag{8}$$

In the focusing system we investigated, the focusing beam is a cylindrical vector axisymmetric QBG beam whose value of the transverse optical field is the same as that of the scalar axisymmetric QBG [12–14], and its polarization distribution is in x direction. Therefore, in the cylindrical coordinate system $(r, \varphi, 0)$, the field distribution $E_0(r, \varphi, z = 0)$ of the axisymmetric QBG beam at the plane $z = 0$ is written in the from [12, 13]

$$E_0(r, \varphi, z = 0) = J_0\left(\frac{\mu r^2}{\omega_0^2}\right)\exp\left(-\frac{r^2}{\omega_0^2}\right) \tag{9}$$

where J_0 denotes the Bessel function of order zero, ω_0 is the waist width of the Gaussian beam, μ is a beam parameter which is complex-valued in general. In order to make focusing properties clear and simplify the calculation process, a simple form of Eq. (9) is made as follow:

$$\begin{aligned} E_0(r, \varphi, z = 0) &= J_0\left(\frac{\mu(r/L)^2}{(\omega_0/L)^2}\right)\exp\left(-\frac{(r/L)^2}{(\omega_0/L)^2}\right) = \\ &= J_0\left(\frac{\mu\sin^2(\theta_1)}{(\omega_0/r_0)^2(r_0/L)^2}\right)\exp\left(-\frac{\sin^2(\theta_1)}{(\omega_0/r_0)^2(r_0/L)^2}\right) \end{aligned} \tag{10}$$

where parameter L is the focal length and r_0 is the radius of incident optical aperture of the focusing optical system. In focusing systems, $\theta_{1\max} = \operatorname{asin}(r_0/L)$. And it is proposed here $w = \omega_0/r_0$ is called the relative waist width. The Eq. (10) can be rewritten as,

$$E_0(\theta_1, z = 0) = J_0\left(\frac{\mu\sin^2(\theta_1)}{w^2\sin^2(\theta_{1\max})}\right)\exp\left(-\frac{\sin^2(\theta_1)}{w^2\sin^2(\theta_{1\max})}\right) \tag{11}$$

where $\theta_1 = \operatorname{asin}(\sin(\theta_2)/n)$ and $\theta_{1m} = \operatorname{asin}(\sin(\theta_{2m})/n) = \alpha$

$$E_0(\theta_2, z = 0) = J_0\left(\frac{\mu\sin^2(\theta_2)}{w^2n^2\sin^2(\alpha)}\right)\exp\left(-\frac{\sin^2(\theta_2)}{w^2n^2\sin^2(\alpha)}\right) \tag{12}$$

The optical intensity in the focal region is proportional to the modulus square of Eq. (1). Basing on the above equations, focusing properties of Weierstrass SIL by an axisymmetric QBG beam can be investigated theoretically.

3. Numerical results and discussions

Without loss of validity and generality, the relative waist width, refractive index of Weierstrass SIL, and maximum convergence angle are chosen as $w = 1$, $n = 2$, $\alpha = 20°$, respectively [21]. And it should be noted that the unit of the focal spot is λ, where λ is the wavelength of the incident beam. Figure 1 gives the intensity distribution in the focal plane of a Weierstrass SIL with clear aperture and $w = 1$, $n = 2$, $\alpha = 20°$. It can be seen from this figure that the focal spot is asymmetric, the transverse focal size in y coordinate direction is very much smaller than that in x coordinate direction, which is also similar to that shown in [21].

Now the intensity distributions in the plane of Weierstrass SIL for different beam parameter μ are calculated and illustrated in Fig. 2. It can be seen that there is only one asymmetric intensity spot in the plane of Weierstrass SIL under condition of small μ, and on increasing μ, the asymmetric intensity spot broadens remarkably, as shown in Fig. 2. When the beam parameter μ increases continuously, the asymmetric intensity spot evolves into one annular intensity distribution, as shown in Figs. 3**a**

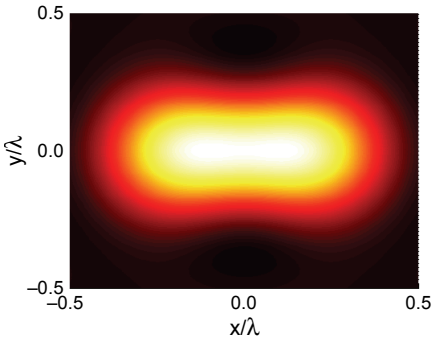

◄ Fig. 1. Intensity distributions in the focal plane of a Weierstrass SIL with clear aperture and $w = 1$, $n = 2$, $\alpha = 20°$.

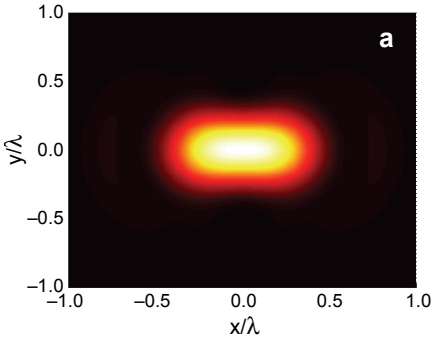

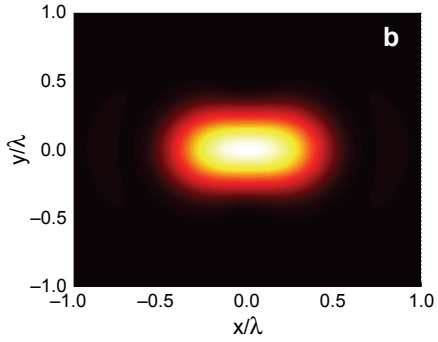

Fig. 2. To be continued on the next page.

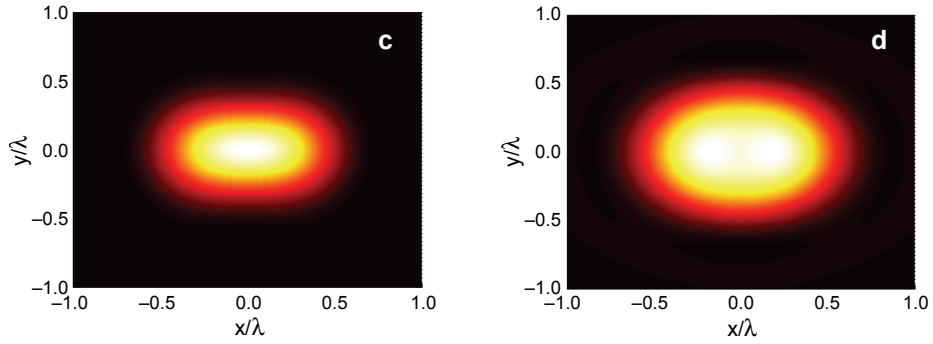

Fig. 2. Intensity distributions in the focal plane of a Weierstrass SIL with different real beam parameter $\mu = 1$ (**a**), $\mu = 2$ (**b**), $\mu = 3$ (**c**), and $\mu = 4$ (**d**).

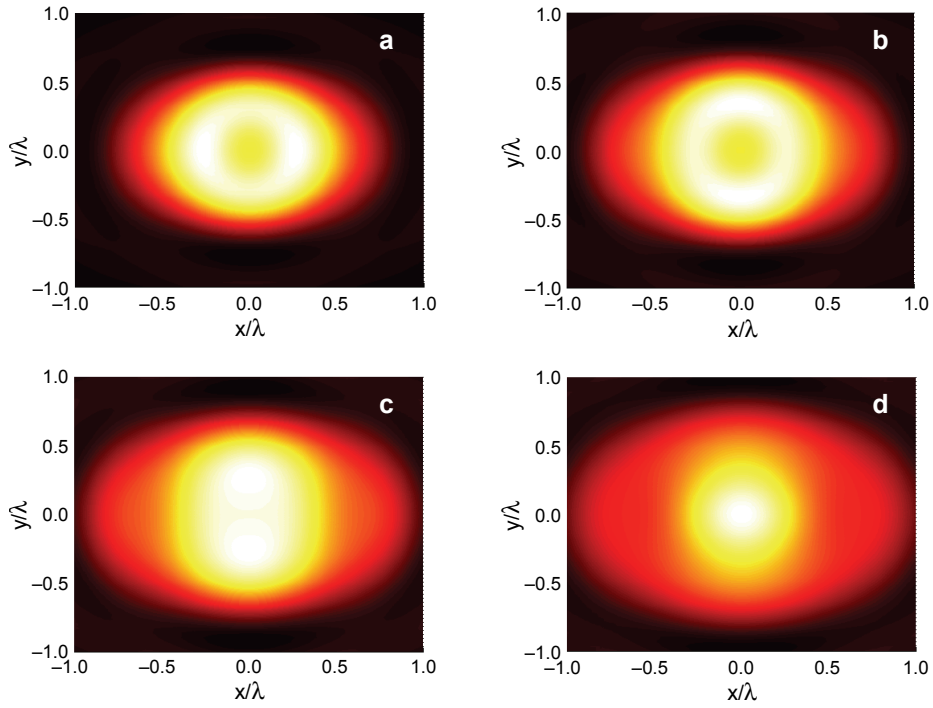

Fig. 3. Intensity distributions in the focal plane of a Weierstrass SIL with different real beam parameter $\mu = 5$ (**a**), $\mu = 6$ (**b**), $\mu = 7$ (**c**), and $\mu = 8$ (**d**).

and 3**b**. For case of higher μ, the annular intensity distribution evolves back into one intensity spot, which is illustrated in Figs. 3**c** and 3**d**. When μ increases continuously, the focal spot also extends remarkably into one annular shaper, and shrinks into one rectangular focal spot with the long axis along x coordinate direction under condition of $\mu = 14$, as shown in Figure 4.

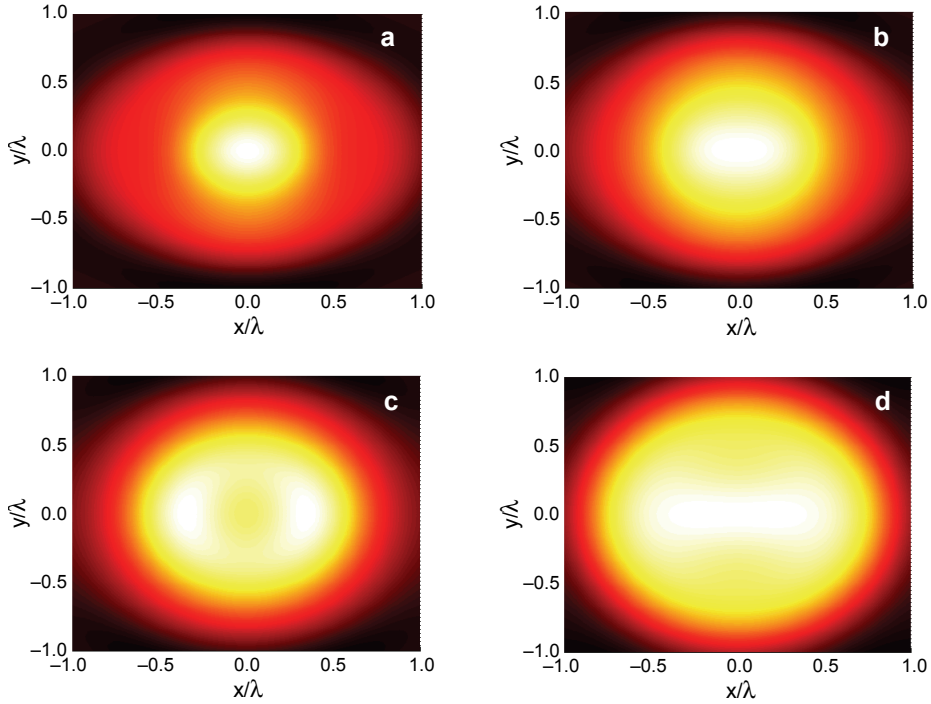

Fig. 4. Intensity distributions in the focal plane of a Weierstrass SIL with different real beam parameter $\mu = 9$ (**a**), $\mu = 10$ (**b**), $\mu = 11$ (**c**), and $\mu = 14$ (**d**).

Intensity distribution curves along x and y coordinates directions in the focal plane of a Weierstrass SIL with different real beam parameter μ are also calculated and shown in Figs. 5 and 6, respectively. It can be seen that the intensity curve along x coordinate firstly extends on increasing μ, then splits into two peaks with increasing distance between these two peaks. When μ increases continuously, the distance between the two peaks decreases so that these two peaks combine back into one peak. On increasing μ continuously, the above process also repeats, as shown in Fig. 5**c**. The similar intensity curve evolution process also happens to that along y coordinate, which is shown in Fig. 6. However, the critical μ of curve splits for that along y coordinate which is bigger than that along x coordinate. For instance, when μ changes from 1 to 4, the intensity curve along y coordinate still turns on one peak, as shown in Figure 6**a**.

It can be seen from Eq. (1) that there are three orthogonal components. And the longitudinal field plays an important role in many optical systems. For instance, the longitudinal field was used to obtain an optical needle that may mean applications in optical data storage density, optical tweezers, and laser machining [22–25]. KOZAWA and co-workers employed the longitudinal field in focal region to enhance the lateral resolution of laser scanning microscopy [26]. In addition, the lateral resolution of laser

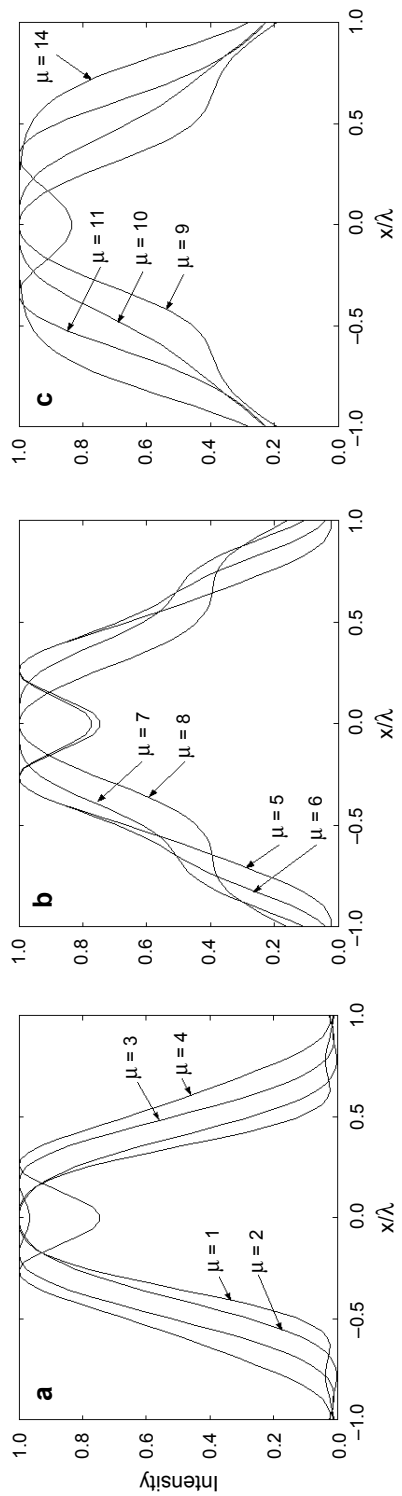

Fig. 5. Intensity distributions curves in x coordinate direction in the focal plane of a Weierstrass SIL with different real beam parameter μ.

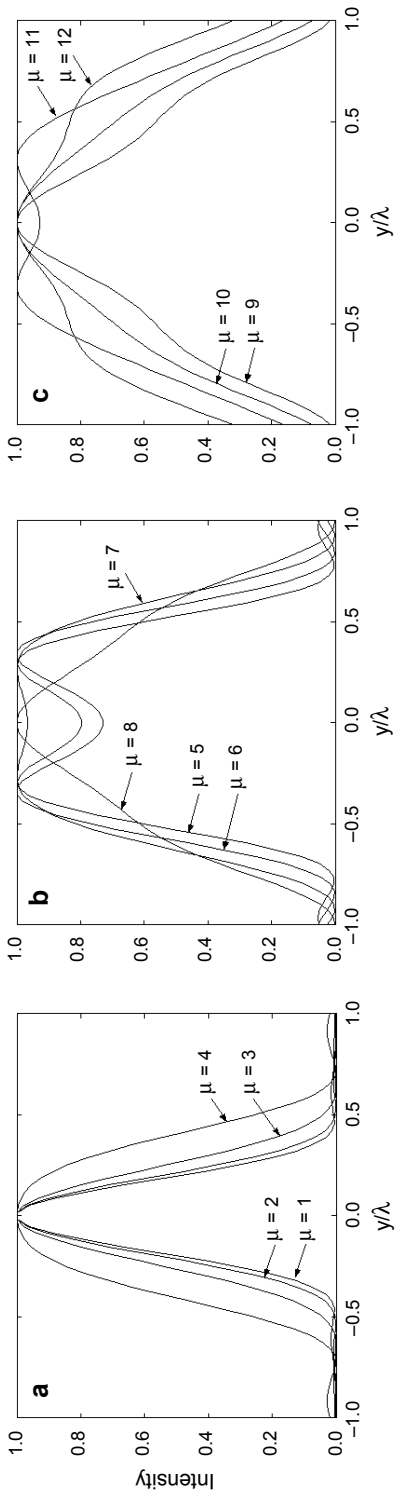

Fig. 6. Intensity distributions curves in y coordinate direction in the focal plane of a Weierstrass SIL with different real beam parameter μ.

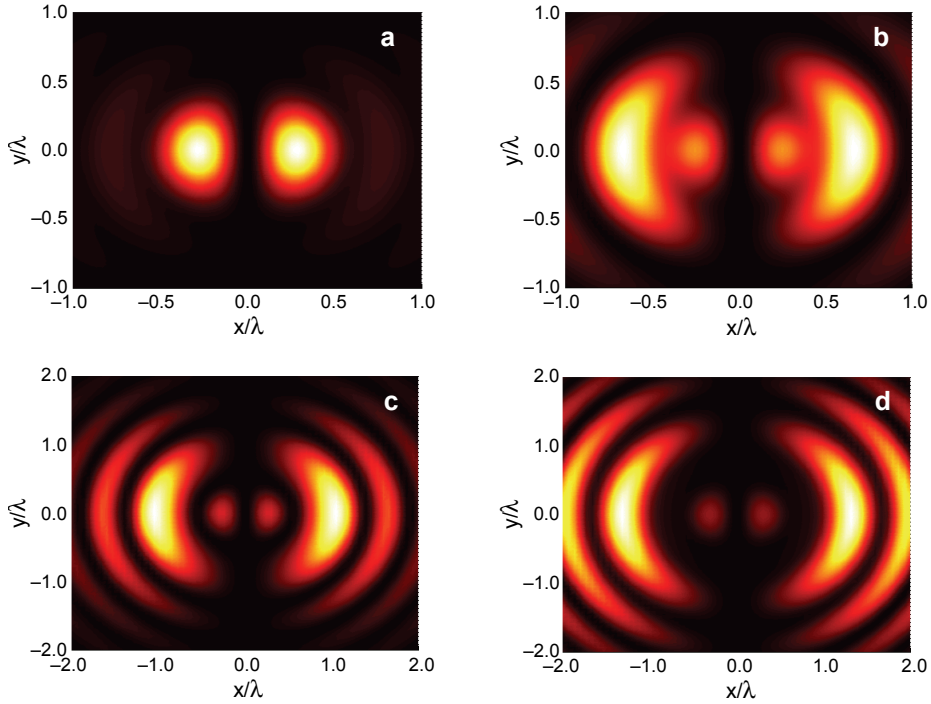

Fig. 7. Intensity distributions of longitudinal field with different real beam parameter $\mu = 1$ (**a**), $\mu = 5$ (**b**), $\mu = 10$ (**c**), and $\mu = 14$ (**d**).

confocal microscopy can also be increased by introducing strong longitudinal component of focal field [27]. Here, we want to illustrate some longitudinal component distributions of the focal field.

Figure 7 shows the intensity distributions of the longitudinal field with different real beam parameter μ. We can see that there are two intensity peaks under condition of $\mu = 1$, as shown in Fig. 7**a**. On increasing μ, these two intensity peaks weaken, and there occur two crescent intensity peaks outside of the center two peaks, as shown in Fig. 7**b**. And when μ increases continuously, the center two peaks weakens considerably, and the crescent intensity peaks shift outward.

The intensity distribution in the focal region of Weierstrass SIL is calculated and shown in Fig. 8. Here only the intensity distributions in y and z coordinates plane are given, namely, $x = 0$. It can be seen from this figure that the intensity maximum locates at the plane of Weierstrass SIL when the parameter μ is small, which is corresponding to Figs. 1 and 2. Under this condition, the Weierstrass SIL can be used to carry out the superresolution effect, in other words, the sharper focal spot can be obtained. However, on increasing μ, the intensity maximum point begins to left the plane of Weierstrass SIL, namely, the focal spot does not locate on the plane of Weierstrass SIL, so the sharper focus disappears. Under this condition, the Weierstrass SIL does not focus the incident beam into a small spot, and the superresolution effect disappears.

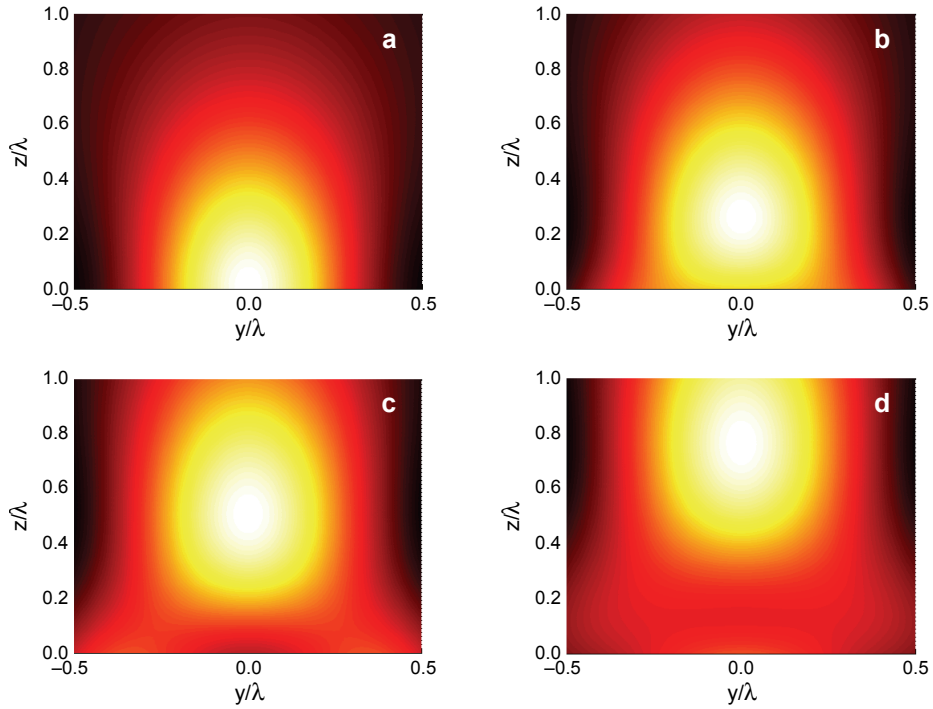

Fig. 8. Intensity distributions in *yoz* plane with different real beam parameter $\mu = 1$ (**a**), $\mu = 2$ (**b**), $\mu = 3$ (**c**), and $\mu = 4$ (**d**).

So the intensity distribution becomes very complex, as shown in Figs. 3 and 4. When the parameter μ increases continuously, the focal spot goes on shifting along the optical axis outside, which is very considerable. Therefore, the incident beam affects the application of Weierstrass SIL to obtain superresolution, and more attention should be paid to use of the Weierstrass SIL.

From Figure 8, we can see that the intensity maximum point shifts far from the plane of the Weierstrass SIL on increasing beam parameter μ. Here the focal shift is investigated in detail. Figure 9 illustrates the dependence of the focal shift on increasing μ. When μ is small, the intensity value decreases continuously on increasing z coordinate, and on increasing μ, the intensity peak lefts from the plane of the Weierstrass SIL continuously. Figure 10 gives the focal shift value curve on increasing μ,

T a b l e 1. Dependence of focal shift value on increasing beam parameter.

μ	0	1	2	3	3.4	3.7	4	5	6
Shift (λ)	0.00	0.00	0.00	0.01	0.13	0.20	0.26	0.39	0.51
μ	7	8	9	10	11	12	13	14	15
Shift (λ)	0.63	0.76	0.89	1.02	1.15	1.29	1.42	1.56	1.70

and Table 1 gives the calculation results. We found that then μ is smaller than 3.4, the focal shift is nearly zero, and then increases sharply on increasing μ. When μ is bigger than 5, the dependence of the focal shift value on increasing μ is nearly linear, which indicates that the parameter μ can be used to alter the focus position.

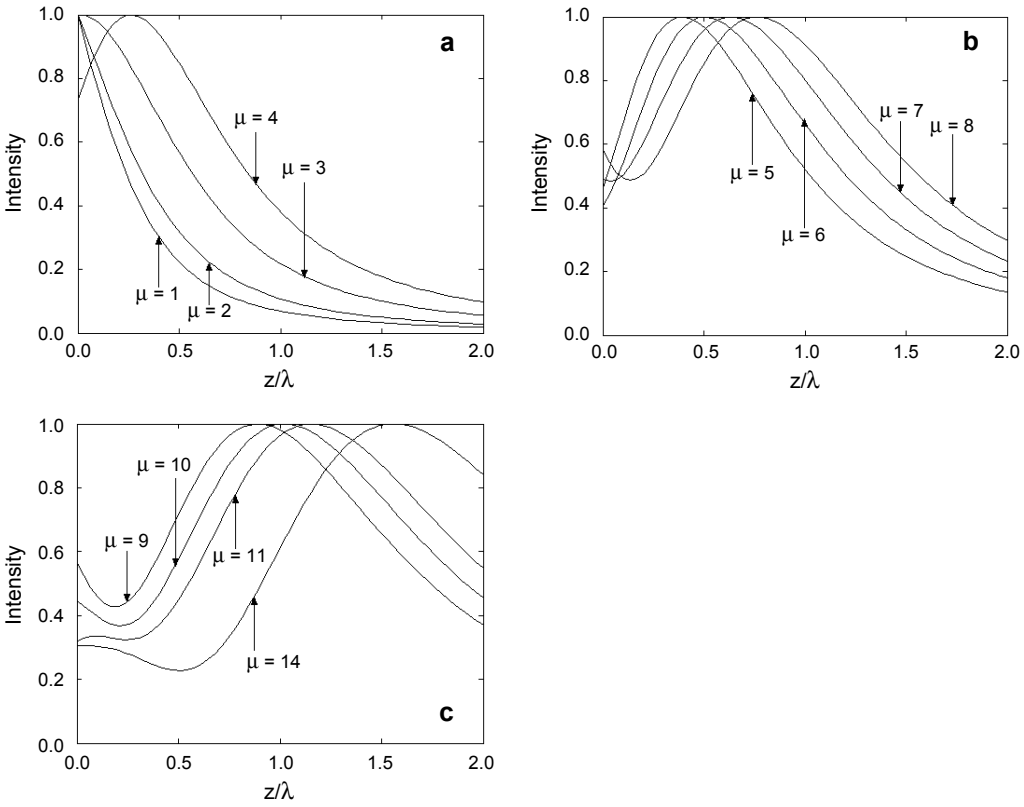

Fig. 9. Intensity distribution curves on the optical axis of a Weierstrass SIL with different real beam parameter μ.

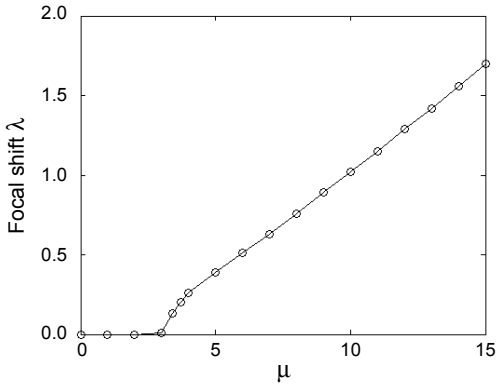

◀ Fig. 10. Dependence of the focal shift on increasing beam parameter μ.

4. Conclusions

In summary, focus shaping of Weierstrass SIL illuminated by an axisymmetric QBG beam is investigated. Results show that sharper focusing of Weierstrass SIL disappears for a certain beam order of QBG beam. For case of a smaller beam order of an axisymmetric QBG beam, the focus still locates on the plane of Weierstrass SIL and Weierstrass SIL can be used to carry out a tighter focusing role. However, when the beam order increases continuously, the focus lefts the plane of Weierstrass SIL, and shifts along the optical axis considerably. In addition, the higher beam order, the dependence of the focal shift on the beam order is nearly linear, which may be used to alter the focal position. Therefore, more attention should be paid to the application of Weierstrass SIL when different incident beams are employed.

Acknowledgements – This work was supported by the National Natural Science Foundation of China (61008044), Shanghai Rising-Star Project (12QA1402300), and the Leading Academic Discipline Project of Shanghai Municipal Government (S30502). Authors thank PhD X. Gao for helpful discussions.

References

[1] WILSON T., SHEPPARD C.J.R., *Theory and Practice of Scanning Optical Microscopy*, Academic, London, 1984.

[2] MANSFIELD S.M., KINO G.S., *Solid immersion microscope*, Applied Physics Letters **57**(24), 1990, pp. 2615–2616.

[3] TERRIS B.D., MAMIN H.J., RUGAR D., STUDENMUND W.R., KINO G.S., *Near-field optical data storage using a solid immersion lens*, Applied Physics Letters **65**(4), 1994, pp. 388–390.

[4] CHEKANOV A., BIRUKAWA M., ITOH Y., SUZUKI T., *"Contact" solid immersion lens near-field optical recording in magneto-optical TbFeCo media*, Journal of Applied Physics **85**(8), 1999, pp. 5324–5326.

[5] GHISLAIN L.P., ELINGS V.B., CROZIER K.B., MANALIS S.R., MINNE S.C., WILDER K., KINO G.S., QUATE C.F., *Near-field photolithography with a solid immersion lens*, Applied Physics Letters **74**(4), 1999, pp. 501–503.

[6] ZWILLER V., BJÖRK G., *Improved light extraction from emitters in high refractive index materials using solid immersion lenses*, Journal of Applied Physics **92**(2), 2002, pp. 660–665.

[7] KARRAI K., LORENZ X., NOVOTNY L., *Enhanced reflectivity contrast in confocal solid immersion lens microscopy*, Applied Physics Letters **77**(21), 2000, pp. 3459–3461.

[8] IPPOLITO S.B., GOLDBERG B.B., ÜNLÜ M.S., *Theoretical analysis of numerical aperture increasing lens microscopy*, Journal of Applied Physics **97**(5), 2005, article 053105.

[9] YOSHITA M., SASAKI T., BABA M., AKIYAMA H., *Application of solid immersion lens to high-spatial resolution photoluminescence imaging of GaAs quantum wells at low temperatures*, Applied Physics Letters **73**(5), 1998, pp. 635–637.

[10] BABA M., SASAKI T., YOSHITA M., AKIYAMA H., *Aberrations and allowances for errors in a hemisphere solid immersion lens for submicron-resolution photoluminescence microscopy*, Journal of Applied Physics **85**(9), 1999, 6923–6925.

[11] WU Q., FEKE G.D., GROBER R.D., GHISLAIN L.P., *Realization of numerical aperture 2.0 using a gallium phosphide solid immersion lens*, Applied Physics Letters **75**(26), 1999, pp. 4064–4066.

[12] CARON C.F.R., POTVLIEGE R.M., *Bessel-modulated Gausian beams with quadratic radial dependence*, Optics Communications **164**(1–3), 1999, pp. 83–93.

[13] HRICHA Z., BELAFHAL A., *Focal shift in the axisymmetric Bessel-modulated Gaussian beam*, Optics Communications **255**(4–6), 2005, pp. 235–240.

[14] WANG X., LÜ B., *The beam propagation factor and far-field distribution of Bessel-modulated Gaussian beams*, Optical and Quantum Electronics **34**(11), 2002, pp. 1071–1077.
[15] BELAFHAL A., DALIL-ESSAKALI L., *Collins formula and propagation of Bessel-modulated Gaussian light beams through an ABCD optical system*, Optics Communications **177**(1–6), 2000, pp. 181–188.
[16] ZHANGRONG MEI, DAOMU ZHAO, XIAOFENG WEI, FENG JING, QIHUA ZHU, *Propagation of Bessel--modulated Gaussian beams through a paraxial ABCD optical system with an annular aperture*, Optik **116**(11), 2005, pp. 521–526.
[17] GAO X., ZHAN Q.F., LI J., HU S., WANG J., ZHUANG S.L., *Cylindrical vector axisymmetric Bessel--modulated Gaussian beam*, Optical and Quantum Electronics **41**(5), 2009, pp. 385–396.
[18] GAO X., ZHAN Q.F., LI J., WANG J., ZHUANG S.L., *Spirally polarized axisymmetric Bessel-modulated Gaussian beam*, Optik **122**(6), 2011, pp. 524–528.
[19] GAO X., ZHAN Q.F., WANG Q., YUN M.J., GUO H.M., ZHUANG S.L., *Subwavelength dark hollow focus of spirally polarized axisymmetric Bessel-modulated Gaussian beam*, European Physical Journal D **64**(1), 2011, pp. 103–108.
[20] HELSETH L.E., *Roles of polarization, phase and amplitude in solid immersion lens systems*, Optics Communications **191**(3–6), 2001, pp. 161–172.
[21] ZHANG Y., YE X., *Three-zone phase-only filter increasing the focal depth of optical storage systems with a solid immersion lens*, Applied Physics B **86**(1), 2007, pp. 97–103.
[22] WANG H., SHI L., LUKYANCHUK B., SHEPPARD C., CHONG TOW CHONG, *Creation of a needle of longitudinally poliatzed light in vacuum using binary optics*, Nature Photonics **2**(8), 2008, pp. 501–505.
[23] SUN C.C., LIU C.K., *Ultrasmall focusing spot with a long depth of focus based on polarization and phase modulation*, Optics Letters **28**(2), 2003, pp. 99–101.
[24] LI X., CAO Y., GU M., *Superresolution-focal-volume induced 3.0 Tbytes/disk capacity by focusing a radially polarized beam*, Optics Letters **36**(13), 2011, pp. 2510–2512.
[25] KAWAUCHI H., YONEZAWA K., KOZAWA Y., SATO S., *Calculation of optical trapping force on a dielectric shpere in the ray optics regime produced by a radially polarized laser beam*, Optics Letters **32**(13), 2007, pp. 1839–1841.
[26] KOZAWA Y., HIBI T., SATO A., HORANAI H., KURIHARA M., HASHIMOTO N., YOKOYAMA H., NEMOTO T., SATO S., *Lateral resolution enhancement of laser scanning microscopy by a higher-order radially polarized mode beam*, Optics Express **19**(17), 2011, pp. 15947–15954.
[27] KIM J., KIM D.C., BACK S.H., *Demonstration of high lateral resolution in laser confocal microscopy using annular and radially polarized light*, Microscopy Research and Technique **72**(6), 2009, pp. 441–446.

Received August 20, 2012
in revised form November 16, 2012